Dynamic polarizabilities and triply magic trapping conditions for $5s^2\ ^1S_0 \rightarrow 5s5p\ ^3P_{0,2}$ transitions of Cd atoms

Ru-Kui Zhang,[1,2] Jun Jiang,[1,*] Chen-Zhong Dong,[1] and Yong-Bo Tang [2,†]

[1]*Key Laboratory of Atomic and Molecular Physics and Functional Materials of Gansu Province, College of Physics and Electronic Engineering, Northwest Normal University, Lanzhou 730070, People's Republic of China*
[2]*Physics Teaching and Experiment Center, Shenzhen Technology University, Shenzhen 518118, People's Republic of China*

The dynamic electric dipole polarizabilities of the $5s^2\ ^1S_0$, $5s5p\ ^3P_0$, and $5s5p\ ^3P_2$ states for Cd atoms are calculated using the relativistic configuration interaction plus many-body perturbation theory method. The magic wavelengths for the $5s^2\ ^1S_0 \rightarrow 5s5p\ ^3P_0$ and $5s^2\ ^1S_0 \rightarrow 5s5p\ ^3P_2$ transitions within a range of 300–500 nm are identified. The possibility of achieving triple magic trapping for the transitions $5s^2\ ^1S_0 \rightarrow 5s5p\ ^3P_0$ and $5s^2\ ^1S_0 \rightarrow 5s5p\ ^3P_2$ is investigated. It is found that no common magic wavelength could be identified for achieving triple magic trapping with the linearly polarized light. However, if the degree of ellipticity is between 0.358 and 1, the triple magic trapping can be achieved at 419.88 nm for the $5s^2\ ^1S_0 \rightarrow 5s5p\ ^3P_2$ ($M_i = \pm 2$) and $5s^2\ ^1S_0 \rightarrow 5s5p\ ^3P_0$ transitions.

I. INTRODUCTION

The development of state-of-the-art optical atomic clocks has made significant progress thanks to advances in laser technologies such as optical frequency combs [1,2], narrow linewidth lasers [3,4], and frequency transmission technologies using optical fibers [5]. Currently, the highest precision of optical clocks is below 10^{-18} [6–9]. To evaluate the performance of optical clocks in experiments, a common approach is to compare two independent clocks to assess their stability, repeatability, and system uncertainty [9–15]. Such comparisons have been made with the same or different types of atoms or ions.

It is known that some ions or atoms, such as Yb [16–19], Yb⁺ [20,21], Al⁺ [22], and Sr [23], possess two long-lived metastable states. Recently, it has been demonstrated that transitions from these metastable states to ground states can be used as clock transitions with very narrow linewidths. This implies that two clock transitions can be measured simultaneously in the same atomic clock. By comparing these two clock transitions within a single atomic clock, it is possible to eliminate system effects and investigate the variation of the fine-structure constant [20–25]. In recent experiments, the optical frequency ratio of the $^2S_{1/2}(F = 0) \rightarrow \ ^2F_{7/2}(F = 3)$ and $^2S_{1/2}(F = 0) \rightarrow \ ^2D_{3/2}(F = 2)$ transitions in ^{171}Yb⁺ was measured by Filzinger *et al.* [21], improving the existing limits on a linear temporal drift of the fine-structure constant [21]; Bohman *et al.* pointed out that the $^1S_0 \rightarrow \ ^3P_2$ transition of the Al⁺ ions is another clock transition and can be used to search for physics beyond the standard model [22]; and Trantmann *et al.* [23] have proposed triple magic trapping in Sr atoms,

where the Stark shifts for the $5s^2\ ^1S_0$, $5s5p\ ^3P_0$, and $5s5p\ ^3P_2$ states are identical, to eliminate the Stark shifts of the two clock transitions.

Cd atoms have two valence electrons, and the $5s^2\ ^1S_0 \rightarrow 5s5p\ ^3P_0$ transition is an ultranarrow clock transition. Cd atoms are promising candidates for compact and transportable optical clocks [26–30]. Yamaguchi *et al.* achieved magic trapping at 419.88(14) nm [29], where the Stark shifts of the $5s^2\ ^1S_0$ and $5s5p\ ^3P_0$ states are equal [31,32]. In theory, there are some works [28,33–36] to calculate the black-body radiation (BBR) shifts, the magic wavelength of the $5s^2\ ^1S_0 \rightarrow 5s5p\ ^3P_0$ clock transition, and the multipolar polarizabilities and hyperpolarizabilities of the $5s^2\ ^1S_0$ and $5s5p\ ^3P_0$ states. Similar to Sr atoms, the $5s5p\ ^3P_2$ state of Cd is also a long-lived metastable state. As shown in Table I, the lifetime of $5s5p\ ^3P_2$ is very close to that of the $5s5p\ ^3P_0$ state. Therefore, the $5s^2\ ^1S_0 \rightarrow 5s5p\ ^3P_2$ transition of Cd can also be considered as a second clock transition. Moreover, the static differential polarizability between $5s^2\ ^1S_0$ and $5s5p\ ^3P_2$ states is similar to that between $5s^2\ ^1S_0$ and $5s5p\ ^3P_0$ states. In addition, the BBR shifts experienced by both the $5s^2\ ^1S_0 \rightarrow 5s5p\ ^3P_0$ and $5s^2\ ^1S_0 \rightarrow 5s5p\ ^3P_2$ transitions are an order of magnitude smaller than those of Sr and Yb lattice clocks operating at the same room temperature [28,37].

In this paper, we employ the relativistic configuration interaction plus second-order many-body perturbation theory (RCI + MBPT) method to calculate the dynamic polarizabilities of the $5s^2\ ^1S_0$ and $5s5p\ ^3P_{0,2}$ states in Cd. The magic wavelengths of the $5s^2\ ^1S_0 \rightarrow 5s5p\ ^3P_{0,2}$ transitions are confirmed based on the dynamic polarizabilities. We then investigate the conditions required for achieving triple magic trapping for the $5s^2\ ^1S_0 \rightarrow 5s5p\ ^3P_0$ and $5s^2\ ^1S_0 \rightarrow 5s5p\ ^3P_2$ transitions near the magic wavelength of 419.88 nm. Throughout this paper, atomic units are used unless otherwise specified.

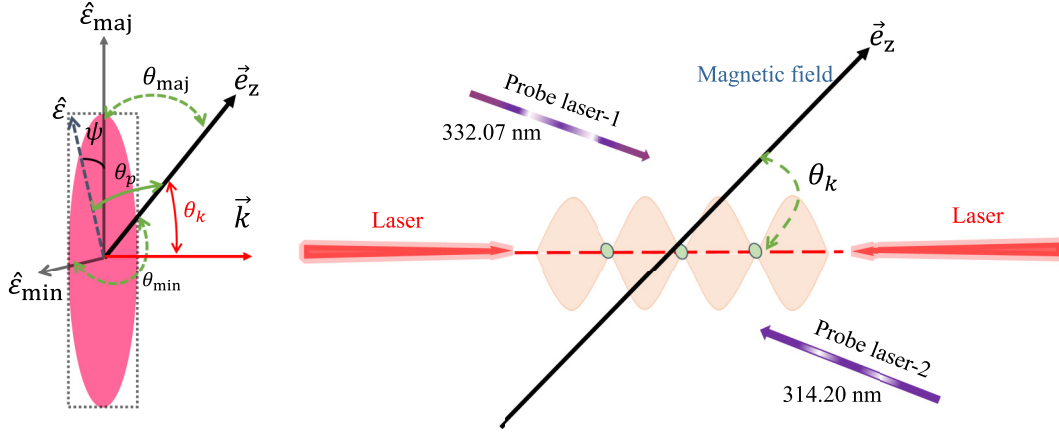*phyjiang@yeah.net
†tangyongbo@sztu.edu.cn

FIG. 1. The schematic of the geometrical parameters of the electromagnetic plane wave and the one-dimensional optical lattice trap. The elliptical area is swept by the electric field vector in one period. The unit vector $\hat{\varepsilon}_{\text{maj}}$ ($\hat{\varepsilon}_{\text{min}}$) is aligned with the semimajor (-minor) axis of the ellipse. $\vec{e}_z$ is the quantization axis, which determines the direction of the magnetic field in the experiment. $\vec{k}$ is the direction of the wave vector. θ_p is the angle between the polarization vector $\hat{\varepsilon}$ and the quantization axis $\vec{e}_z$, and θ_k is the angle between $\vec{e}_z$ and $\vec{k}$. Here $\hat{\varepsilon}_{\text{maj}}$, $\hat{\varepsilon}_{\text{min}}$, and $\vec{k}$ are orthogonal to each other. θ_{maj} (θ_{min}) is the angle between $\hat{\varepsilon}_{\text{maj}}$ ($\hat{\varepsilon}_{\text{min}}$) and $\vec{e}_z$. ψ is directly related to the degree of circular polarization of the electromagnetic plane wave. Probe laser 1 and Probe laser 2 represent two probe lasers with wavelengths of 332.07 and 314.20 nm of the two clock transitions $5s^2\ {}^1S_0 \rightarrow 5s5p\ {}^3P_0$ and $5s^2\ {}^1S_0 \rightarrow 5s5p\ {}^3P_2$, respectively.

II. THEORY

A. The expression of the polarizabilities

When an ion or atom exposed to a laser field with the laser frequency ω, degree of ellipticity $\mathcal{A}$, and direction of the wave vector $\vec{k}$, as shown in Fig. 1, the energy shift due to the Stark effect can be written as [40]

$$\Delta E_i = -\frac{1}{2}\alpha_i(\omega)F^2 + \cdots, \quad (1)$$

where $\alpha_i(\omega)$ is the dynamic dipole polarizability of the quantum state i, and F is a measure of the strength of the ac electromagnetic field. The dipole polarizability can be calculated using the sum-over-states method, and the general expression of dynamic dipole polarizability can be written as [40–43]

$$\alpha_i(\omega) = \alpha_i^S(\omega) + \mathcal{A}\cos\theta_k\frac{M_i}{2J_i}\alpha_i^V(\omega)$$

$$+ \frac{3\cos^2\theta_p - 1}{2}\frac{3M_i^2 - J_i(J_i+1)}{J_i(2J_i-1)}\alpha_i^T(\omega), \quad (2)$$

where M_i is the component of the total angular momentum J_i. θ_k is the angle between $\vec{e}_z$ and $\vec{k}$, $\vec{e}_z$ is the quantization axis (the direction of static magnetic field), and $\cos\theta_k = \vec{k}\cdot\vec{e}_z$. Geometrically, θ_p is related to θ_{maj} and θ_{min}, it can be written as

$$\cos^2\theta_p = \cos^2\psi\cos^2\theta_{\text{maj}} + \sin^2\psi\cos^2\theta_{\text{min}}$$

$$= \sin^2\psi\sin^2\theta_k + \cos(2\psi)\cos^2\theta_{\text{maj}}. \quad (3)$$

Here, θ_{maj} (θ_{min}) is the angle between the major (minor) axis of the ellipse and the $\vec{e}_z$ axis. For linearly polarized light, θ_p is the angle between the laser polarization vector $\hat{\varepsilon}$ and the $\vec{e}_z$ axis. The degree of ellipticity $\mathcal{A}$ is directly related to the angle ψ ($|\psi| \leqslant 45°$),

$$\mathcal{A} = \sin 2\psi. \quad (4)$$

$\mathcal{A} = 0$ is linearly polarized light, and $\mathcal{A} = +1$ and -1 are the right-handed and left-handed circularly polarized light, respectively. $\alpha_i^S(\omega)$, $\alpha_i^V(\omega)$, and $\alpha_i^T(\omega)$ are the scalar, vector, and tensor polarizabilities, and they can be expressed as

$$\alpha_i^S(\omega) = \frac{2}{3(2J_i+1)}\sum_n \frac{\varepsilon_{\text{in}}\langle\gamma_nJ_n\|d\|\gamma_iJ_i\rangle^2}{\varepsilon_{\text{in}}^2 - \omega^2}, \quad (5)$$

$$\alpha_i^V(\omega) = -2\sqrt{\frac{6J_i}{(J_i+1)(2J_i+1)}}$$

$$\times \sum_n (-1)^{J_i+J_n}\begin{Bmatrix} 1 & 1 & 1 \\ J_i & J_i & J_n \end{Bmatrix}\frac{\omega\langle\gamma_nJ_n\|d\|\gamma_iJ_i\rangle^2}{\varepsilon_{\text{in}}^2 - \omega^2}, \quad (6)$$

and

$$\alpha_i^T(\omega) = 4\left(\frac{5J_i(2J_i-1)}{6(J_i+1)(2J_i+1)(2J_i+3)}\right)^{1/2}$$

$$\times \sum_n (-1)^{J_i+J_n}\begin{Bmatrix} J_i & 1 & J_n \\ 1 & J_i & 2 \end{Bmatrix}\frac{\langle\gamma_nJ_n\|d\|\gamma_iJ_i\rangle^2\varepsilon_{\text{in}}^2}{\varepsilon_{\text{in}}^2 - \omega^2}, \quad (7)$$

where $\varepsilon_{\text{in}} = E_n - E_i$ is excitation energy, and $\langle\gamma_nJ_n\|d\|\gamma_iJ_i\rangle$ is the reduced $E1$ transition matrix element. If $\omega = 0$, the dynamic polarizabilities in Eqs. (5) and (7) are reduced to the static polarizabilities, and the static vector polarizability equals 0.

The dynamic polarizability of the Cd^{2+} core is calculated using a pseudospectral oscillator strength distribution method, similar to that used in Refs. [44–47]. Table II lists the pseudospectral oscillator strength distribution for Cd^{2+}, where the pseudo-oscillator strength f_n is equal to the number of electrons in the shell. The excitation energy is set by adding a constant to the Koopman energies and adjusting the constant until the core polarizability, calculated from the

TABLE I. The lifetimes (in seconds) of the $5s5p\ ^3P_2$ and $5s5p\ ^3P_0$ states of Cd [38].

Atom	$\tau(5s5p\ ^3P_2)$	$\tau(5s5p\ ^3P_0)$
[111]Cd	19.0	17.9
[113]Cd	18.0	16.1

oscillator strength sum rule, matches the known core polarizability 4.97 a.u. [40,48,49].

B. RCI + MBPT Method

The wave functions and energy levels of Cd are obtained by the RCI + MBPT calculation. In this method, the many-electron atomic or ionic system is divided into a frozen core part and valence electron parts. The initial step is to perform a self-consistent Dirac-Fock (DF) calculation to obtain all the single-particle orbitals. These orbitals are then used to build the configuration space. In this step, we use the no-pair Dirac Hamiltonian and treat both the Coulomb and the Breit interactions on an equal footing, similar to Refs. [50–52]. The next step involves carrying out second-order many-body perturbation and configuration interaction calculations to account for the core-valence and valence-valence correlations.

The effective interaction equation for the divalent atomic system can be expressed as

$$\left\{ \sum_i^2 [H_{\mathrm{DF}}(r_i) + \Sigma_1(r_i)] + \left(\frac{1}{r_{12}} + \Sigma_2 \right) \right\} |\gamma J\rangle = E |\gamma J\rangle, \tag{8}$$

where H_{DF} and $\frac{1}{r_{12}}$ denote the DF Hamiltonian and the electron-electron Coulomb interaction, respectively. Σ_1 is the one-body correlation potential, which describes the correlation interaction between a valence electron and the core. The Σ_2 represents the two-body correlation potential, which describes the screening of the Coulomb interaction between valence electrons and the core electrons. The matrix elements of the one-body and two-body correlation potentials are given in Ref. [53]. To account for the correlation effects beyond the second order, we introduce the rescaling parameter ρ_κ and substitute the one-body correlation potentials Σ_1 with $\rho_\kappa \Sigma_1$

in practice. The rescaling parameter ρ_κ is tuned to reproduce the experimental energy of the lowest state for each angular quantum number κ of a monovalent atomic system, which is similar to the Dirac-Fock plus core polarization (DFCP) method [50]. The rescaling parameter can accelerate the convergence of the RCI + MBPT method.

For the transition matrix element calculation, it is necessary to consider the core polarization correction. In present work, we take the core polarization correction into account by using the random phase approximation [54,55]. Further details on the RCI + MBPT method can be found in Refs. [53,56–60].

In the DF calculation, the large and small components of the Dirac wave functions are expanded using 50 B-spline bases of order $k = 13$ and the box size $R_{\mathrm{max}} = 240$. The partial waves are limited to $\ell_{\mathrm{max}} = 5$ and the lowest 40 orbital sets of each partial wave are used to construct the configuration space. In the second-order many-body perturbation calculations, the summation is carried out over the entire basis set. The rescaling parameters are $\rho_{-1} = 0.902$, $\rho_1 = 0.971$, $\rho_{-2} = 0.982$, $\rho_2 = 1.028$, $\rho_{-3} = 1.037$, and $\rho_{\mathrm{others}} = 1.0$, respectively.

III. RESULTS AND DISCUSSION

A. Energy levels, reduced $E1$ matrix elements, and static polarizabilities

Table III lists the presently calculated energy levels and compares them with the National Institute of Standards and Technology (NIST) tabulations [39]. Our RCI + MBPT results are in excellent agreement with the NIST results, especially for the low-lying states such as the $5s^2\ ^1S_0$, $5s5p\ ^3P_0$, $^3P_1$, and $^3P_2$ states, with differences of only 0.05%, 0.02%, 0.02%, and 0.03%, respectively. For other excited states, the largest discrepancy does not exceed 0.5%.

Table IV presents the reduced matrix elements for some of the main transitions and compares them with other available results. The present results for the transitions from the $5s^2\ ^1S_0$ state agree well with those of the configuration interaction plus an all-order linearized coupled-cluster (CI + All) method [29], the configuration interaction plus many-body perturbation theory (CI + MBPT) [28,29], and the DFCP method [36]; the differences are about 1%, 1%, and 2%, respectively. For the transitions from the $5s5p\ ^3P_0$ state, the differences between the present results with these three methods are about 0.3%, 0.5%, and 2.5%, respectively. Regarding the transitions from the $5s5p\ ^3P_1$, $5s5p\ ^3P_2$, and $5s5p\ ^1P_1$ states, there are no other theoretical results available for comparison. However, all of the present results are in agreement with those of the NIST [39]. Table V lists the results of the static dipole polarizabilities of the $5s^2\ ^1S_0$, $5s5p\ ^3P_{0,1,2}$, and $5s5p\ ^1P_1$ states. In the present calculations, the experimental transition energies are used for the low-lying excited states. The numbers of the intermediate states are $N_{J^P=1^+} = 10\,457$, $N_{J^P=1^-} = 10\,140$, $N_{J^P=2^+} = 14\,390$, and $N_{J^P=3^+} = 15\,077$, where $+$ and $-$ represent even and odd parity, respectively. For the $5s^2\ ^1S_0$ state, the present static polarizability of 47.4(1.5) a.u. is in excellent agreement with the experimental value of 47.5(2.0) a.u. [62]. The

TABLE II. Pseudospectral oscillator strength distribution for Cd^{2+} ions. The transition energies $\Delta E^2_{n \to i}$ are given in a.u.

n	$\Delta E^2_{n \to i}$	f_n
1	961625.7331	2.0
2	20777.9141	2.0
3	565.0139	2.0
4	0.6154	2.0
5	352.5699	6.0
6	132.0840	6.0
7	5.5682	6.0
8	67.3807	10.0
9	23.0199	10.0

TABLE III. Comparison of energy levels (in cm^{-1}) for some low-lying states. All the energies are given relative to the ground state of the Cd^{2+} core. The relative differences between the present energy and the NIST energy [39] are listed as Diff.

State	Present	NIST [39]	Diff.
$5s^2\ ^1S_0$	-208818.3	-208914.8	0.05%
$5s5p\ ^3P_0^o$	-178829.2	-178800.8	0.02%
$5s5p\ ^3P_1^o$	-178291.1	-178258.7	0.02%
$5s5p\ ^3P_2^o$	-177138.6	-177087.8	0.03%
$5s5p\ ^1P_1^o$	-166007.0	-165222.4	0.47%
$5s6s\ ^3S_1$	-157917.5	-157430.8	0.31%
$5s6s\ ^1S_0$	-156035.7	-155604.7	0.28%
$5s6p\ ^3P_0^o$	-151075.4	-150523.9	0.37%
$5s6p\ ^3P_1^o$	-151004.8	-150453.2	0.37%
$5s6p\ ^3P_2^o$	-150829.1	-150279.1	0.37%
$5s5d\ ^1D_2$	-150217.9	-149695.0	0.35%
$5s5d\ ^3D_1$	-150019.9	-149429.0	0.40%
$5s5d\ ^3D_2$	-150008.7	-149416.9	0.40%
$5s6p\ ^1P_1^o$	-149642.4	-149007.5	0.43%
$5s7s\ ^3S_1$	-146945.8	-146351.3	0.41%
$5s7s\ ^1S_0$	-146398.1	-145827.9	0.39%
$5s7p\ ^3P_0^o$	-144522.3	-143918.9	0.42%
$5s7p\ ^3P_1^o$	-144496.1	-143889.3	0.42%
$5s7p\ ^3P_2^o$	-144427.7	-143821.1	0.42%
$5s6d\ ^1D_2$	-144364.5	-143780.0	0.41%
$5s6d\ ^3D_1$	-144184.8	-143561.4	0.43%
$5s6d\ ^3D_2$	-144179.6	-143555.9	0.43%
$5s7p\ ^1P_1^o$	-144044.6	-143413.4	0.44%
$5s4f\ ^3F_2^o$	-143971.2	-143328.7	0.45%
$5s8s\ ^3S_1$	-142854.1	-142232.7	0.44%
$5s8s\ ^1S_0$	-142618.6	-142009.1	0.43%
$5s8p\ ^3P_0^o$	-141710.1	-141085.1	0.44%
$5s7d\ ^1D_2$	-141686.2	-141076.4	0.43%
$5s8p\ ^3P_2^o$	-141663.3	-141039.6	0.44%
$5s7d\ ^3D_1$	-141557.7	-140925.0	0.45%
$5s7d\ ^3D_2$	-141554.9	-140922.1	0.45%
$5s5f\ ^3F_2^o$	-141461.7	-140821.1	0.45%
$5s9s\ ^1S_0$	-140740.4	-140116.0	0.45%
$5s9p\ ^3P_0^o$	-140232.2	-139600.7	0.45%

FIG. 2. The dynamical polarizabilities of the $5s^2\ ^1S_0$ and $5s5p\ ^3P_0$ states in the 300–500 nm wavelength range. The vertical dashed lines indicate the positions of the resonant transitions. The magic-zero wavelengths (λ_0) are determined by locating points where either $5s5p\ ^3P_0$ or $5s^2\ ^1S_0$ polarizabilities are equal to zero and the magic wavelengths (λ_m) are determined by locating points where the $5s5p\ ^3P_0$ and $5s^2\ ^1S_0$ polarizabilities are equal to each other. They are all identified by arrows.

For the $5s5p\ ^3P_0$ state, the differences between the present calculations and the other theoretical results are within 3%. As for the $5s5p\ ^3P_1$, $5s5p\ ^3P_2$, and $5s5p\ ^1P_1$ states, it is found that the present results are in agreement with the results of the RCCSD calculations [64]. The tensor polarizability of the $5s5p\ ^3P_1$ state, 7.74(22) a.u., is in good agreement with the experimental value of 7.11(32) a.u. [65].

It should be noted that the differential polarizabilities $\alpha(5s5p\ ^3P_0) - \alpha(5s^2\ ^1S_0)$ and $\alpha(5s5p\ ^3P_2\ M_i = \pm 2) - \alpha(5s^2\ ^1S_0)$ are 29.9(2.8) and 21.1(2.5) a.u., respectively, as shown in Table VI. The difference between these two values is small. This means that at the same temperature the BBR shift of the $5s^2\ ^1S_0 \rightarrow 5s5p\ ^3P_2\ M_i = \pm 2$, transition is similar to that of the $5s^2\ ^1S_0 \rightarrow 5s5p\ ^3P_0$ transition.

B. The magic wavelengths for linearly polarized light

For linearly polarized light, that is, $\psi = 0$ and $\mathcal{A} = 0$, Eq. (2) can be simplified as

$$\alpha_i(\omega) = \alpha_i^S(\omega) + \frac{3\cos^2\theta_p - 1}{2} \frac{3M_i^2 - J_i(J_i + 1)}{J_i(2J_i - 1)} \alpha_i^T(\omega), \quad (9)$$

where θ_p satisfies $0 \leqslant \cos^2\theta_p \leqslant 1$. For states with $J_i \geqslant 1$, the polarizabilities include the scalar and tensor components, which are associated with M_i and θ_p. For $J_i = 0$ states, however, the polarizabilities are determined only by the scalar component.

Figure 2 shows the dynamic polarizabilities of the $5s^2\ ^1S_0$ and $5s5p\ ^3P_0$ states. Three magic wavelengths for the $5s^2\ ^1S_0 \rightarrow 5s5p\ ^3P_0$ transition are found and identified by arrows. The longest magic wavelength obtained from our results is 420.20(57) nm, which agrees well with the experimental measurement of 419.88(14) nm [29] and theoretical calculations of 420.1(7) nm using the CI + All approach

differences between the present results and the CI + All and CI + MBPT results are about 0.9 a.u. These differences are mainly due to the difference in the reduced matrix elements, as shown in Table IV. If we replace the present reduced matrix element of the $5s^2\ ^1S_0 \rightarrow 5s5p\ ^1P_1$ transition, which dominantly contributes to the polarizability of the $5s^2\ ^1S_0$ state, with the CI + All value of 3.440 [29] or the CI + MBPT value of 3.435 a.u. [28], the corresponding values become 46.17 and 46.38 a.u., respectively. The differences between the present results and the results of the relativistic coupled-cluster theory (RCC) [35], the DFCP method [36], and the relativistic coupled-cluster single-double excitations approach (RCCSD) [64] are about 1.4 a.u. These differences are mainly caused by the difference in reduced matrix elements and transition energies. The uncertainties given in this table are determined by introducing 2% changes in the dominant matrix elements, since most of the present results agree with other results within 2%.
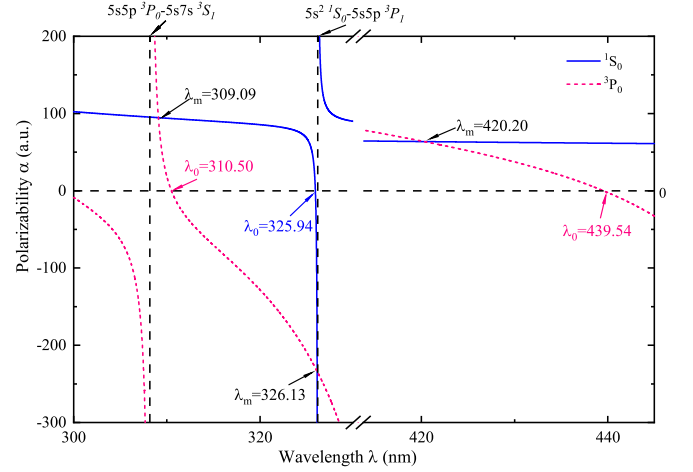
TABLE IV. Comparison of some reduced $E1$ matrix elements (in a.u.) for principal transitions of Cd. The numbers in the parentheses are uncertainties.

Transition	Present	CI + All [29]	CI + MBPT	DFCP [36]	Expt.[c] [39]
$5s^2\ ^1S_0 \to 5s5p\ ^1P_1$	3.479	3.440	3.426 [29]	3.4787[a]	3.01
			3.435 [28]	3.4292[b]	
$5s^2\ ^1S_0 \to 5s5p\ ^3P_1$	0.167		0.158 [28]		0.14
$5s^2\ ^1S_0 \to 5s6p\ ^1P_1$	0.670	0.689	0.675 [29]	0.5957[a]	
				0.6552[b]	
$5s5p\ ^3P_0 \to 5s6s\ ^3S_1$	1.493	1.491	1.502 [29]	1.6085[a]	1.42
			1.486 [28]	1.5619[b]	
$5s5p\ ^3P_0 \to 5s5d\ ^3D_1$	2.325	2.318	2.306 [29]	2.4537[a]	2.12
			2.222 [28]	2.3667[b]	
$5s5p\ ^3P_0 \to 5s7s\ ^3S_1$	0.433	0.433	0.432 [29]	0.4479[a]	
				0.4445[b]	
$5s5p\ ^3P_0 \to 5s6d\ ^3D_1$	1.066	1.061	1.062 [29]	1.0998[a]	0.97
				1.0778[b]	
$5s5p\ ^3P_1 \to 5s5d\ ^3D_2$	3.543				3.51
$5s5p\ ^3P_1 \to 5s6s\ ^3S_1$	2.642				2.58
$5s5p\ ^3P_1 \to 5s5d\ ^3D_1$	2.044				2.03
$5s5p\ ^3P_2 \to 5s5d\ ^3D_3$	5.045				4.63
$5s5p\ ^3P_2 \to 5s6s\ ^3S_1$	3.592				3.30
$5s5p\ ^3P_2 \to 5s5d\ ^3D_2$	2.128				2.03
$5s5p\ ^1P_1 \to 5s5d\ ^1D_2$	5.427				6.23
$5s5p\ ^1P_1 \to 5s6s\ ^1S_0$	3.923				

[a]Represents the values obtained without including the high-order one-body and two-body core-polarization potentials.
[b]Represents the values obtained with the high-order one-body and two-body core-polarization potentials.
[c]The values of the experimental matrix elements are obtained from the oscillator strengths.

[29] and 420 nm calculated using the CPMP approach [33]. The number in parentheses represents the uncertainty of the magic wavelength. The uncertainty was primarily caused by the uncertainty of the dominant matrix elements. In the present work, we change the dominant matrix elements by 2% separately to calculate the change of the magic wavelength. Subsequently, the uncertainty of the magic wavelength is determined as the root mean square of each change. There

TABLE V. Comparison of the static dipole polarizabilities (a.u.) of the low-lying states of Cd with available experimental and theoretical results. Numbers in parentheses represent the uncertainties in the last digits. The polarizability of the core in the present work is $\alpha_{core} = 4.97$ a.u. [40,48,49].

	α^S			α^T		
	Present	Refs.	Expt.	Present	Refs.	Expt.
$5s^2\ ^1S_0$	47.4(1.5)	46.53 CI + All [29]	49.65(165) [61]			
		46.52 CI + MBPT [28]	47.5(2.0) [62]			
		46.02(50) RCC [35]				
		46.9 DHF [63]				
		46(2) DFCP [36]				
		45.92(10) RCCSD [64]				
		44.63 CPMP [33]				
$5s5p\ ^3P_0$	77.3(2.3)	76.2 CI + All [29]				
		78(6) DFCP [36]				
		75.31 CI + MBPT [28]				
		75.03(42) RCCSD [64]				
		75.29 CPMP [33]				
$5s5p\ ^3P_1$	80.2(2.2)	77.87(40) RCCSD [64]		7.74(33)	7.30(7) RCCSD [64]	7.11(32) [65]
					6.30 Model potential [66]	5.35(16) [67]
						6.91 [68]
						6.83(28) [69]
$5s5p\ ^3P_2$	87.7(1.8)	84.82(34) RCCSD [64]		−19.15(84)	−18.05(13) RCCSD [64]	
$5s5p\ ^1P_1$	218.0(6.2)	225.18(2.59) RCCSD [64]		−84.9(2.6)	−90.99(1.75) RCCSD [64]	

TABLE VI. Comparison of the differential polarizabilities $\Delta\alpha(^3P_0 - {}^1S_0)$ and $\Delta\alpha(^3P_2 - {}^1S_0)$. The total polarizability $\alpha(5s5p\,^3P_2)$ is calculated by letting $\alpha_i^V = 0$ and $\theta_p = 0°$ in Eq. (2).

$\Delta\alpha$	Present	Refs.
$\Delta\alpha(^3P_0 - {}^1S_0)$	29.9(2.8)	29.67 CI + All [29]
		28.79 CI + MBPT [28]
		29.11(43) RCCSD [64]
		30.66 CPMP [33]
$\Delta\alpha(^3P_2 - {}^1S_0)$		
$M_i = \pm 2$	21.1(2.5)	20.85(38) RCCSD [64]
$M_i = \pm 1$	49.9(2.5)	47.93(38) RCCSD [64]
$M_i = 0$	59.4(2.5)	56.95(38) RCCSD [64]

are no comparable theoretical or experimental results for the other two magic wavelengths, 326.13(1) and 309.09(2) nm. These two magic wavelengths have difficulties trapping Cd atoms, because they are very close to the resonance wavelengths of the $5s^2\,^1S_0 \to 5s5p\,^3P_1$ and $5s5p\,^3P_0 \to 5s7s\,^3S_1$ transitions, which are 326.20 and 308.17 nm, respectively.

Figure 3 shows the dynamic polarizabilities of the $5s^2\,^1S_0$ state and each of the magnetic sublevels of the $5s5p\,^3P_2$ state for the case $\theta_p = 0°$. The magic wavelengths, denoted by arrows, are listed in Table VII. It can be seen that there are two magic wavelengths for each of the magnetic sublevel transitions of $5s^2\,^1S_0 \to 5s5p\,^3P_2$ $|M_i| = 0, 1, 2$. These magic wavelengths lie within two resonance intervals. The magic wavelengths near 300 nm lie between the resonance wavelengths of the $5s5p\,^3P_2 \to 5s7s\,^3S_1$ and $5s5p\,^3P_2 \to 5s6d\,^1D_2$ transitions. The longest magic wavelengths for each of these transitions lie between the resonance wavelengths of the $5s5p\,^3P_2 \to 5s6s\,^3S_1$ and $5s5p\,^3P_2 \to 5s5d\,^1D_2$ transitions.

It is worth noting that these longest magic wavelengths are located in the same resonance transition region as the 419.88-nm magic wavelength of the $5s^2\,^1S_0 \to 5s5p\,^3P_0$ transition. This is a crucial requirement for finding a common magic wavelength to achieve triple magic trapping for both the $5s^2\,^1S_0 \to 5s5p\,^3P_0$ and $5s^2\,^1S_0 \to 5s5p\,^3P_2$ clock transitions. Additionally, it should be noted that when $\theta_p = 0°$ there is no magic wavelength for the $5s^2\,^1S_0 \to 5s5p\,^3P_2$ $|M_i| = 2$ transition in this range. This is due to the cancellation

TABLE VII. Magic wavelengths of the $5s^2\,^1S_0 \to 5s5p\,^3P_2$ transition in the case of the magnetic field being vertical to the wave vector $\vec{k}$ with the linearly polarized light, that is, $\cos^2\theta_p = 1$ and $\mathcal{A} = 0$.

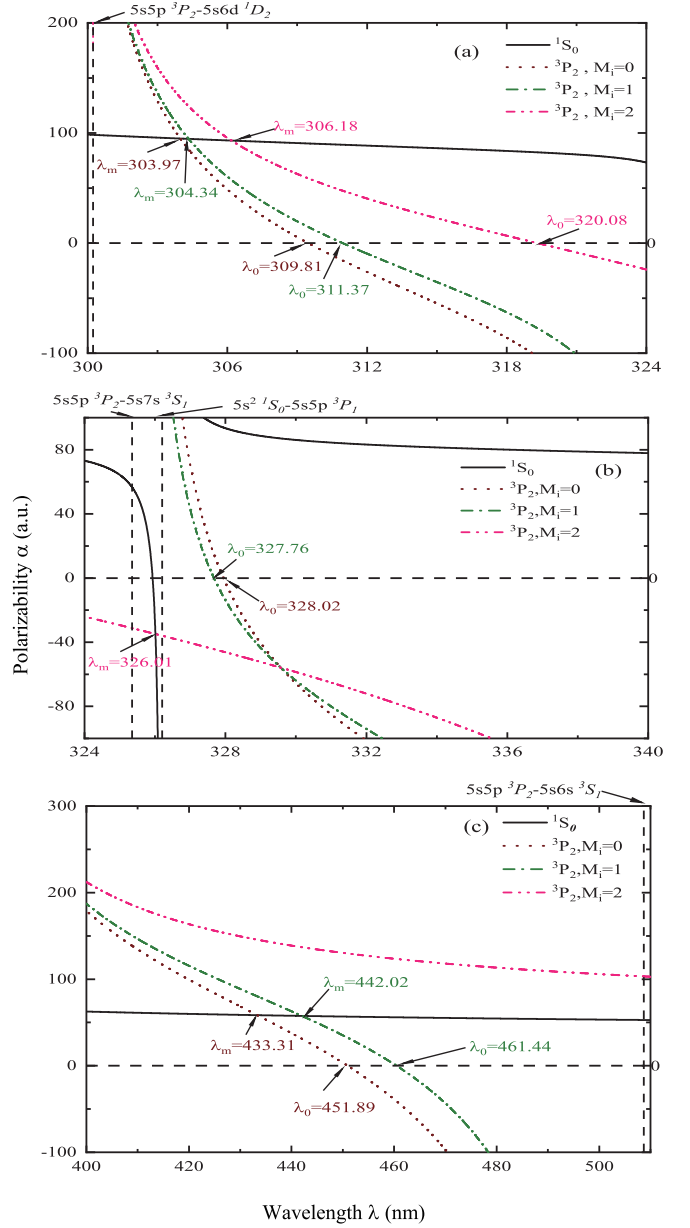| Resonances	λ_{res}	$|M_i| = 0$	$|M_i| = 1$	$|M_i| = 2$
$5s5p\,^3P_2 \to 5s6s\,^3S_1$	508.72			
		433.31(97)	442.0(1.4)	
$5s5p\,^3P_2 \to 5s5d\,^1D_2$	365.06			
$5s5p\,^3P_2 \to 5s5d\,^3D_1$	361.55			
				326.01(2)
$5s5p\,^3P_2 \to 5s7s\,^3S_1$	325.35			
		303.97(15)	304.34(25)	306.18(25)
$5s5p\,^3P_2 \to 5s6d\,^1D_2$	300.23			

FIG. 3. The dynamical polarizabilities of $^1S_0$ and $^3P_2$ states. The vertical dashed lines indicate the positions of the resonant transitions and are given on the top of the figures. The magic wavelengths (λ_m) are determined by locating points where the $5s5p\,^3P_2$ and $5s^2\,^1S_0$ polarizabilities are equal to each other, and the magic-zero wavelength (λ_0) of a state is determined when the polarizability is zero. They are all identified by arrows.

of the contribution of the tensor and scalar terms of the $5s5p\,^3P_2 \to 5s6s\,^3S_1$ transition to the dynamic polarizability of the $5s5p\,^3P_2$ $|M_i| = 2$ states. As a result, the polarizability of $5s5p\,^3P_2$ $|M_i| = 2$ changes slowly near the $5s5p\,^3P_2 \to 5s6s\,^3S_1$ resonance wavelength, as shown in Fig. 3(c).

Figure 4 shows the variation of the longest magic wavelength of the $5s^2\,^1S_0 \to 5s5p\,^3P_2$ $M_i = 0, 1, 2$ transitions with the angle θ_p. In the range of $0° \leqslant \theta_p \leqslant 90°$, the magic wavelength for the $M_i = 0$ and 1 transitions exhibits a monotonically increasing trend. The minimum values are 433.31
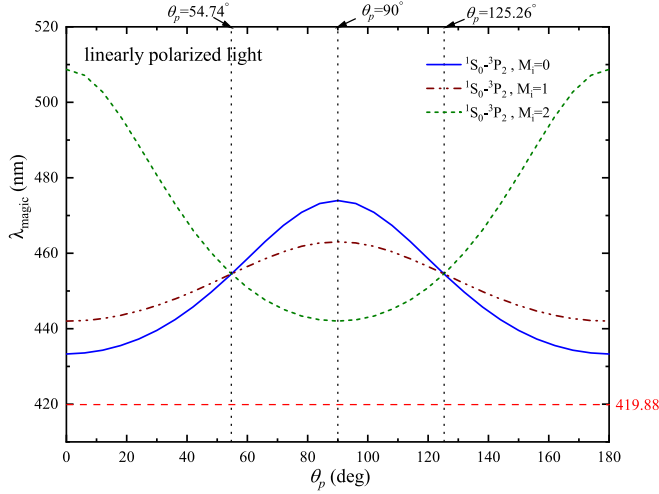
FIG. 4. The variation of the longest magic wavelengths with θ_p under the linearly polarized light for the $5s^2\,{}^1S_0 \to 5s5p\,{}^3P_2$ transition.
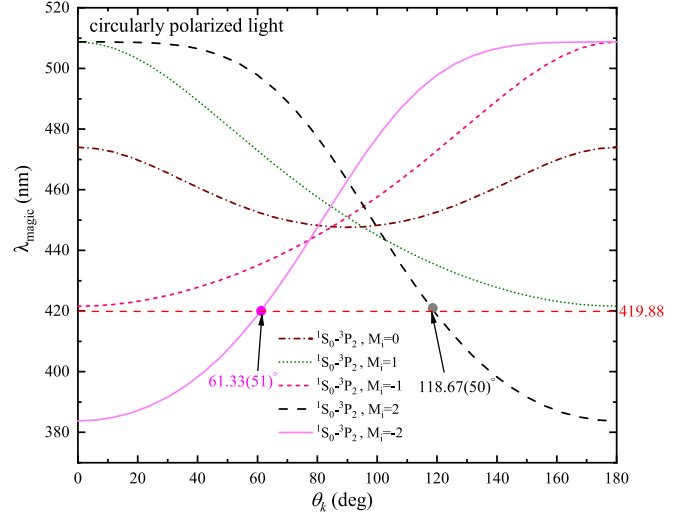

FIG. 5. θ_k-dependent magic wavelengths under the circularly polarized light for the $5s^2\,{}^1S_0 \to 5s5p\,{}^3P_2$ transition. The triply magic trapping conditions are indicated by dots.

and 442.0 nm at $\theta_p = 0°$ for the $M_i = 0$ and 1 transitions, respectively. However, for the $M_i = 2$ transition, the magic wavelength decreases with increasing angle θ_p, and reaches a minimum value of 442 nm at $\theta_p = 90°$. Therefore, all of these magic wavelengths are greater than 419.88 nm. Consequently, it is not possible to find a common magic wavelength that can achieve triple magic trapping for the $5s^2\,{}^1S_0 \to 5s5p\,{}^3P_0$ and $5s^2\,{}^1S_0 \to 5s5p\,{}^3P_2$ transitions.

C. Magic wavelengths for circularly polarized light

According to Eq. (2), the dynamic polarizabilities for the negative M_i states with left-handed polarized light are the same as those of the positive M_i state with right-handed polarized light. For this reason, in the following discussion we only give the polarizabilities of the $5s5p\,{}^3P_2$ $M_i = 0, 1, 2$ states for right-handed polarized light.

For the right-handed circularly polarized light, $\psi = \pi/4$, $\mathcal{A} = 1$, and $\cos^2\theta_p = \frac{1}{2}\sin^2\theta_k$, and Eq. (2) can be expressed as

$$\alpha_i(\omega) = \alpha_i^S(\omega) + \frac{\cos\theta_k M_i}{2J_i}\alpha_i^V(\omega)$$
$$+ \frac{\frac{3}{2}\sin^2\theta_k - 1}{2}\frac{3M_i^2 - J_i(J_i + 1)}{J_i(2J_i - 1)}\alpha_i^T(\omega), \quad (10)$$

where the polarizability depends on M_i and θ_k due to the contribution of the vector and tensor components $\alpha_i^V(\omega)$ and $\alpha_i^T(\omega)$.

When $\theta_k = 90°$, the polarizabilities for circularly polarized light are the same as those for linearly polarized light. Therefore, the magic wavelength should be the same for both cases. Figure 5 depicts the dependence of the longest magic wavelength for the magnetic sublevel transitions of $5s^2\,{}^1S_0 \to 5s5p\,{}^3P_2$ $M = 0, 1, 2$ on the angle θ_k. We can see that the magic wavelengths for the transitions from the $M_i = 0$ and ± 1 states are all greater than 419.88 nm. However, it is worth noting that the magic wavelengths of the $M_i = +2$ and -2 transitions are 419.88 nm at $\theta_k = 61.33(51)°$ and 118.67(50)°, respectively. This implies that 419.88 nm is a

common magic wavelength for the $5s^2\,{}^1S_0 \to 5s5p\,{}^3P_0$ and $5s^2\,{}^1S_0 \to 5s5p\,{}^3P_2$ $M_i = \pm 2$ transitions to achieve triple magic trapping.

D. The triple magic trapping conditions for elliptically polarized light

According to Eqs. (2) and (3), for the elliptically polarized light, the polarizability of the $5s5p\,{}^3P_2$ state can be expressed as

$$\alpha_i(\omega) = \alpha_i^S(\omega) + \mathcal{A}\frac{\cos\theta_k M_i}{2J_i}\alpha_i^V(\omega)$$
$$+ \frac{3\left(\frac{1 - \sqrt{1 - \mathcal{A}^2}}{2}\sin^2\theta_k + \sqrt{1 - \mathcal{A}^2}\cos^2\theta_{\mathrm{maj}}\right) - 1}{2}$$
$$\times \frac{3M_i^2 - J_i(J_i + 1)}{J_i(2J_i - 1)}\alpha_i^T(\omega), \quad (11)$$

where the polarizability for each of the magnetic sublevels depends on $\mathcal{A}$, θ_k, and θ_{maj}. Therefore, the magic wavelength of the clock transition of $5s^2\,{}^1S_0 \to 5s5p\,{}^3P_2$ depends on these three parameters as well.

We have made a thorough analysis of the variation of the longest magic wavelength for each magnetic sublevel transition of the $5s^2\,{}^1S_0 \to 5s5p\,{}^3P_2$ $M = 0, 1, 2$ transitions with respect to these three parameters. For the $5s^2\,{}^1S_0 \to 5s5p\,{}^3P_2$ $|M_i| = 0, 1$ transitions, the magic wavelength is always greater than 420 nm. However, for the $5s^2\,{}^1S_0 \to 5s5p\,{}^3P_2$ $M_i = \pm 2$ sublevel transitions, the variation of the longest magic wavelength is more significant as these parameters change. Interestingly, we find that 419.88 nm is a common magic wavelength for the $5s^2\,{}^1S_0 \to 5s5p\,{}^3P_0$ and $5s^2\,{}^1S_0 \to 5s5p\,{}^3P_2$ $M_i = \pm 2$ transitions when these three
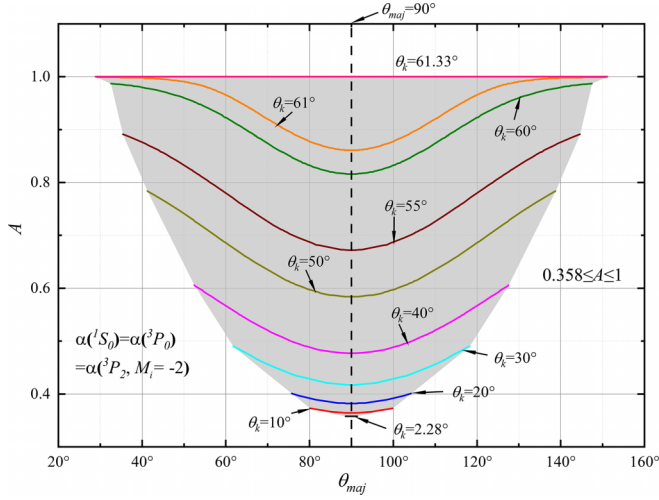
FIG. 6. Triple magic trapping conditions for $5s^2\ ^1S_0 \rightarrow 5s5p\ ^3P_0$ and $5s^2\ ^1S_0 \rightarrow 5s5p\ ^3P_2\ M_i = -2$ clock transitions in the case of the elliptically polarized light at the 419.88-nm magic wavelength. The gray area represents the three parameters $\mathcal{A}$, θ_k, and θ_{maj} satisfying the conditions of the triple magic trapping.

parameters satisfy the relation

$$
70.9079 = 76.5011 M_i \mathcal{A}\cos\theta_k + 32.3004
$$
$$
\times \frac{3\left(\frac{1-\sqrt{1-\mathcal{A}^2}}{2}\sin^2\theta_k + \sqrt{1-\mathcal{A}^2}\cos^2\theta_{\text{maj}}\right) - 1}{2},
$$
(12)

where $M_i = \pm 2$. In this equation, the theoretical dynamic polarizabilities $\alpha^S_{^1S_0}(\omega)$, $\alpha^S_{^3P_2}(\omega)$, $\alpha^V_{^3P_2}(\omega)$, and $\alpha^T_{^3P_2}(\omega)$ at $\lambda = 419.88$ nm are used.

In Fig. 6, the gray area represents the range where triple magic trapping at 419.88 nm can be achieved for the $5s^2\ ^1S_0 \rightarrow 5s5p\ ^3P_0$ and $5s^2\ ^1S_0 \rightarrow 5s5p\ ^3P_2\ M_i = -2$ clock transitions under right-handed elliptically polarized light. The solid lines indicate the corresponding values of θ_k for the triple magic trap. It can be seen that triple magic trapping can be achieved within $0.358 \leqslant \mathcal{A} \leqslant 1$, and $2.28° \leqslant \theta_k \leqslant 61.33°$. For left-handed elliptically polarized light ($\mathcal{A} < 0$), the triple magic condition for the $M_i = -2$ transition is symmetrical to that of right-handed light ($\mathcal{A} > 0$) with respect to the direction of $\theta_k = 90°$, i.e., θ_k should satisfy $180° - 2.28° \geqslant \theta_k \geqslant 180° - 61.33°$. For the $M_i = 2$ transition, the triple magic condition is the same as for the $5s^2\ ^1S_0 \rightarrow 5s5p\ ^3P_2\ M_i = -2$ transition, except for the opposite polarization $\mathcal{A}$.

To make the experiment easier to perform, we suggest setting the angle θ_{maj} to $90°$, i.e., the direction of the magnetic field lies within the plane formed by the $\hat{\varepsilon}_{\text{min}}$ and $\vec{k}$ axes. In this case, triple magic trapping can be achieved by adjusting only the angle θ_k, as shown in Fig. 7. $\mathcal{A}$ and θ_k satisfy the following equation:

$$
87.0581 = 76.5011 M_i \mathcal{A}\cos\theta_k
$$
$$
+ 24.2253(1 - \sqrt{1-\mathcal{A}^2})\sin^2\theta_k. \quad (13)
$$

Here, $\mathcal{A}$ should be within the range of $0.358 \leqslant |\mathcal{A}| \leqslant 1$. For right-handed light, the range for the angle θ_k is $2.28° \leqslant$
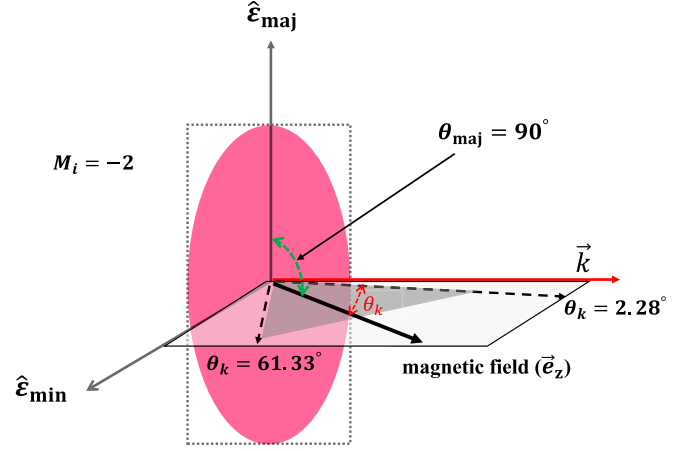

FIG. 7. Representation of the triple magic trapping conditions when $\theta_{\text{maj}} = 90°$. The magnetic field $\vec{e}_z$ rotates in the plane composed of $\hat{\varepsilon}_{\text{min}}$ and $\vec{k}$. The gray area indicates the range of magnetic field directions within which the triple magic trapping condition can be achieved under the elliptically polarized light for the $5s^2\ ^1S_0 \rightarrow 5s5p\ ^3P_0$ and $5s^2\ ^1S_0 \rightarrow 5s5p\ ^3P_2\ M_i = -2$ transitions at the longest magic wavelength.

$\theta_k \leqslant 61.33°$ (indicated by the gray area in the figure) for the $5s^2\ ^1S_0 \rightarrow 5s5p\ ^3P_2\ M_i = -2$ transition and $180° - 2.28° \geqslant \theta_k \geqslant 180° - 61.33°$ for the $5s^2\ ^1S_0 \rightarrow 5s5p\ ^3P_2\ M_i = 2$ transition. The range of θ_k for left-handed light can be determined by its symmetry with right-handed light.

Finally, we evaluated the sensitivity coefficient [70,71] for the $5s^2\ ^1S_0 \rightarrow 5s5p\ ^3P_0$ and $5s^2\ ^1S_0 \rightarrow 5s5p\ ^3P_2$ transitions: $q \approx \frac{\omega(+\delta)-\omega(-\delta)}{2\delta}$, where ω is the transition energy and δ is the change of the fine-structure constant. In these estimates, we changed the fine-structure constant by 0.1% and recalculated the excitation energies of the $5s^2\ ^1S_0 \rightarrow 5s5p\ ^3P_0$ and $5s^2\ ^1S_0 \rightarrow 5s5p\ ^3P_2$ transitions. The sensitivity coefficients for these two transitions are 5000 and 8150 cm^{-1}, respectively, and the enhancement factors [70,71], $K = \frac{2q}{\omega}$, are 0.388 and 0.299, respectively. The difference between these sensitivities is small.

IV. CONCLUSIONS

The energy levels and the reduced $E1$ transition matrix elements of Cd atoms are calculated using the RCI + MBPT method. The static and dynamic dipole polarizabilities of the $5s^2\ ^1S_0$, $5s5p\ ^1P_1$, and $5s5p\ ^3P_{0,1,2}$ states are then determined by the sum-over-states method. The present results are in good agreement with the available theoretical and experimental results. Since the $5s5p\ ^3P_2$ state is also a long-lived metastable state, the $5s^2\ ^1S_0 \rightarrow 5s5p\ ^3P_2$ transition can also be considered as a second clock transition. The static differential polarizability between the $5s^2\ ^1S_0$ and $5s5p\ ^3P_2\ M_i = \pm 2$ states is close to that between the $5s^2\ ^1S_0$ and $5s5p\ ^3P_0$ states. The magic wavelengths for the $5s^2\ ^1S_0 \rightarrow 5s5p\ ^3P_0$ and $5s^2\ ^1S_0 \rightarrow 5s5p\ ^3P_2$ transitions are identified. The presently calculated magic wavelength of 420.20(57) nm for the $5s^2\ ^1S_0 \rightarrow 5s5p\ ^3P_0$ transition is in good agreement with the experimental value of 419.88 nm [29] and other theoretical results [33].

In addition, we analyze the common magic wavelengths for the clock transitions $5s^2\ ^1S_0 \rightarrow 5s5p\ ^3P_0$ and $5s^2\ ^1S_0 \rightarrow 5s5p\ ^3P_2$ under linearly, circularly, and elliptically polarized light. While no common magic wavelength is found for linearly polarized light, it is observed that, for $0.358 \leqslant |\mathcal{A}| \leqslant 1$, 419.88 nm can be used as a common magic wavelength for the $5s^2\ ^1S_0 \rightarrow 5s5p\ ^3P_0$ and $5s^2\ ^1S_0 \rightarrow 5s5p\ ^3P_2\ M_i = \pm 2$ transitions to achieve triple magic trapping. We suggest that by setting the angle θ_{maj} to $90°$, triple magic trapping can be achieved by adjusting only the angle between the direction of the static magnetic field and the direction of the wave vector $\vec{k}$ (i.e., θ_k). Overall, our results provide valuable insights into the properties of Cd atoms and the potential for clock transitions at specific wavelengths under different types of light polarization.

[1] T. Udem, R. Holzwarth, and T. W. Hänsch, Nature (London) **416**, 233 (2002).

[2] S. T. Cundiff and J. Ye, Rev. Mod. Phys. **75**, 325 (2003).

[3] B. C. Young, F. C. Cruz, W. M. Itano, and J. C. Bergquist, Phys. Rev. Lett. **82**, 3799 (1999).

[4] D. G. Matei, T. Legero, S. Häfner, C. Grebing, R. Weyrich, W. Zhang, L. Sonderhouse, J. M. Robinson, J. Ye, F. Riehle, and U. Sterr, Phys. Rev. Lett. **118**, 263202 (2017).

[5] F. Riehle, Nat. Photon. **11**, 25 (2017).

[6] S. L. Campbell, R. Hutson, G. Marti, A. Goban, N. Darkwah Oppong, R. McNally, L. Sonderhouse, J. Robinson, W. Zhang, B. Bloom, and J. Ye, Science **358**, 90 (2017).

[7] E. Oelker, R. Hutson, C. Kennedy, L. Sonderhouse, T. Bothwell, A. Goban, D. Kedar, C. Sanner, J. Robinson, G. Marti, D. G. Matei, T. Legero, M. Giunta, R. Holzwarth, F. Riehle, U. Sterr, and J. Ye, Nat. Photon. **13**, 714 (2019).

[8] S. M. Brewer, J. S. Chen, A. M. Hankin, E. R. Clements, C. W. Chou, D. J. Wineland, D. B. Hume, and D. R. Leibrandt, Phys. Rev. Lett. **123**, 033201 (2019).

[9] X. Zheng, J. Dolde, V. Lochab, B. N. Merriman, H. Li, and S. Kolkowitz, Nature (London) **602**, 425 (2022).

[10] B. J. Bloom, T. L. Nicholson, J. R. Williams, S. L. Campbell, M. Bishof, X. Zhang, W. Zhang, S. L. Bromley, and J. Ye, Nature (London) **506**, 71 (2014).

[11] T. Kobayashi, A. Takamizawa, D. Akamatsu, A. Kawasaki, A. Nishiyama, K. Hosaka, Y. Hisai, M. Wada, H. Inaba, T. Tanabe, and M. Yasuda, Phys. Rev. Lett. **129**, 241301 (2022).

[12] I. Ushijima, M. Takamoto, M. Das, T. Ohkubo, and H. Katori, Nat. Photon. **9**, 185 (2015).

[13] R. Tyumenev, M. Favier, S. Bilicki, E. Bookjans, R. L. Targat, J. Lodewyck, D. Nicolodi, Y. L. Coq, M. Abgrall, J. Guéna, L. D. Sarlo, and S. Bize, New J. Phys. **18**, 113002 (2016).

[14] N. Ohmae, F. Bregolin, N. Nemitz, and H. Katori, Opt. Express **28**, 15112 (2020).

[15] M. E. Kim, W. F. McGrew, N. V. Nardelli, E. R. Clements, Y. S. Hassan, X. Zhang, J. L. Valencia, H. Leopardi, D. B. Hume, T. M. Fortier, A. D. Ludlow, and D. R. Leibrandt, Nat. Phys. **19**, 25 (2023).

[16] M. S. Safronova, S. G. Porsev, C. Sanner, and J. Ye, Phys. Rev. Lett. **120**, 173001 (2018).

[17] V. A. Dzuba, V. V. Flambaum, and S. Schiller, Phys. Rev. A **98**, 022501 (2018).

[18] T. Ishiyama, K. Ono, T. Takano, A. Sunaga, and Y. Takahashi, Phys. Rev. Lett. **130**, 153402 (2023).

[19] Z. M. Tang, Y. M. Yu, B. K. Sahoo, C. Z. Dong, Y. Yang, and Y. M. Zou, Phys. Rev. A **107**, 053111 (2023).

[20] R. Lange, N. Huntemann, J. M. Rahm, C. Sanner, H. Shao, B. Lipphardt, C. Tamm, S. Weyers, and E. Peik, Phys. Rev. Lett. **126**, 011102 (2021).

[21] M. Filzinger, S. Dörscher, R. Lange, J. Klose, M. Steinel, E. Benkler, E. Peik, C. Lisdat, and N. Huntemann, Phys. Rev. Lett. **130**, 253001 (2023).

[22] M. A. Bohman, S. G. Porsev, D. B. Hume, D. R. Leibrandt, and M. S. Safronova, Phys. Rev. A **108**, 053120 (2023).

[23] J. Trautmann, D. Yankelev, V. Klüsener, A. J. Park, I. Bloch, and S. Blatt, Phys. Rev. Res. **5**, 013219 (2023).

[24] R. M. Godun, P. B. R. Nisbet-Jones, J. M. Jones, S. A. King, L. A. M. Johnson, H. S. Margolis, K. Szymaniec, S. N. Lea, K. Bongs, and P. Gill, Phys. Rev. Lett. **113**, 210801 (2014).

[25] M. G. Raizen, G. Gilbert, and D. Budker, Phys. Rev. A **106**, 032209 (2022).

[26] V. D. Ovsiannikov, V. G. Pal'chikov, A. V. Taichenachev, V. I. Yudin, H. Katori, and M. Takamoto, Phys. Rev. A **75**, 020501 (2007).

[27] Y. Kaneda, J. M. Yarborough, Y. Merzlyak, A. Yamaguchi, K. Hayashida, N. Ohmae, and H. Katori, Opt. Lett. **41**, 705 (2016).

[28] V. A. Dzuba and A. Derevianko, J. Phys. B **52**, 215005 (2019).

[29] A. Yamaguchi, M. S. Safronova, K. Gibble, and H. Katori, Phys. Rev. Lett. **123**, 113201 (2019).

[30] M. Takamoto, Y. Tanaka, and H. Katori, Appl. Phys. Lett. **120**, 140502 (2022).

[31] J. Ye, D. W. Vernooy, and H. J. Kimble, Phys. Rev. Lett. **83**, 4987 (1999).

[32] H. Katori, T. Ido, and M. Kuwata-Gonokami, J. Phys. Soc. Jpn. **68**, 2479 (1999).

[33] A. Ye and G. Wang, Phys. Rev. A **78**, 014502 (2008).

[34] S. G. Porsev and M. S. Safronova, Phys. Rev. A **102**, 012811 (2020).

[35] B. K. Sahoo and Y. M. Yu, Phys. Rev. A **98**, 012513 (2018).

[36] M. Zhou and L. Y. Tang, Chin. Phys. B **30**, 083102 (2021).

[37] S. G. Porsev and A. Derevianko, Phys. Rev. A **74**, 020502 (2006).

[38] A. P. Mishra and T. Balasubramanian, J. Quant. Spectrosc. Radiat. Transfer **69**, 769 (2001).

[39] A. Kramida, Yu. Ralchenko, J. Reader, and NIST ASD Team, NIST Atomic Spectra Database, National Institute of Standards

and Technology, Gaithersburg, MD, 2022, available at https://physics.nist.gov/asd.

[40] J. Mitroy, M. S. Safronova, and C. W. Clark, J. Phys. B **43**, 202001 (2010).

[41] N. L. Manakov, V. D. Ovsiannikov, and L. P. Rapoport, Phys. Rep. **141**, 320 (1986).

[42] K. Beloy, Theory of the AC Stark Effect on the Atomic Hyperfine Structure and Applications to Microwave Atomic Clocks, Ph.D thesis, University of Nevada, Reno, 2009.

[43] F. Le Kien, P. Schneeweiss, and A. Rauschenbeutel, Eur. Phys. J. D **67**, 92 (2013).

[44] J. Jiang, L. Y. Tang, and J. Mitroy, Phys. Rev. A **87**, 032518 (2013).

[45] J. Mitroy and M. W. J. Bromley, Phys. Rev. A **68**, 052714 (2003).

[46] D. J. Margoliash and W. J. Meath, J. Chem. Phys. **68**, 1426 (1978).

[47] A. Kumar and W. J. Meath, Mol. Phys. **54**, 823 (1985).

[48] W. Johnson, D. Kolb, and K. N. Huang, At. Data Nucl. Data Tables **28**, 333 (1983).

[49] M. Aymar, C. H. Greene, and E. Luc-Koenig, Rev. Mod. Phys. **68**, 1015 (1996).

[50] Y. B. Tang, H. X. Qiao, T. Y. Shi, and J. Mitroy, Phys. Rev. A **87**, 042517 (2013).

[51] Y. B. Tang, C. B. Li, and H. X. Qiao, Chin. Phys. B **23**, 063101 (2014).

[52] Y. B. Tang, B. Q. Lou, and T. Y. Shi, Phys. Rev. A **96**, 022513 (2017).

[53] M. S. Safronova, M. G. Kozlov, W. R. Johnson, and D. Jiang, Phys. Rev. A **80**, 012516 (2009).

[54] V. A. Dzuba, V. V. Flambaum, M. G. Kozlov, and S. G. Porsev, J. Exp. Theor. Phys. **87**, 885 (1998).

[55] I. M. Savukov and W. R. Johnson, Phys. Rev. A **62**, 052512 (2000).

[56] V. A. Dzuba, V. V. Flambaum, and M. G. Kozlov, Phys. Rev. A **54**, 3948 (1996).

[57] V. A. Dzuba and W. R. Johnson, Phys. Rev. A **57**, 2459 (1998).

[58] S. G. Porsev, M. G. Kozlov, Y. G. Rakhlina, and A. Derevianko, Phys. Rev. A **64**, 012508 (2001).

[59] I. M. Savukov and W. R. Johnson, Phys. Rev. A **65**, 042503 (2002).

[60] R. K. Zhang, J. Jiang, C. Z. Dong, and Y. B. Tang, Phys. Rev. A **108**, 012803 (2023).

[61] D. Goebel and U. Hohm, Phys. Rev. A **52**, 3691 (1995).

[62] U. Hohm, Opt. Spectrosc. **130**, 290 (2022).

[63] B. O. Roos, R. Lindh, P. Å. Malmqvist, V. Veryazov, and P. O. Widmark, J. Phys. Chem. A **109**, 6575 (2005).

[64] X. T. Guo, Y. M. Yu, Y. Liu, B. B. Suo, and B. K. Sahoo, Phys. Rev. A **103**, 013109 (2021).

[65] R. H. Rinkleff, Z. Phys. A: Hadrons Nucl. **291**, 23 (1979).

[66] E. J. Robinson, J. Opt. Soc. Am. **59**, 782 (1969).

[67] S. Legowski, A. Molhem, G. Osiński, and P. Rudecki, Z. Phys. D: At. Mol. Clusters **35**, 101 (1995).

[68] A. M. Bonch-Bruevich and V. A. Khodovoî, Sov. Phys. Usp. **10**, 637 (1968).

[69] A. Khadjavi, A. Lurio, and W. Happer, Phys. Rev. **167**, 128 (1968).

[70] V. V. Flambaum and V. A. Dzuba, Can. J. Phys. **87**, 25 (2009).

[71] M. G. Kozlov, M. S. Safronova, J. R. Crespo López-Urrutia, and P. O. Schmidt, Rev. Mod. Phys. **90**, 045005 (2018).